

Energy spectra of exciton states in disk-shaped GaAs-Ga_{1-x}Al_xAs quantum dots under growth-direction magnetic fields

Z. Barticevic¹, M. Pacheco¹, C.A. Duque^{2,a}, and L.E. Oliveira³

¹ Departamento de Física, Universidad Técnica Federico Santa María, Casilla 110-V, Valparaíso, Chile

² Instituto de Física, Universidad de Antioquia, AA 1226, Medellín, Colombia

³ Instituto de Física, Unicamp, CP 6165, Campinas - SP, 13083-970, Brazil

Received 31 October 2006 / Received in final form 11 April 2007

Published online 16 May 2007 – © EDP Sciences, Società Italiana di Fisica, Springer-Verlag 2007

Abstract. A theoretical study, within the effective-mass approximation, of the effects of applied magnetic fields on excitons in disk-shaped GaAs-Ga_{1-x}Al_xAs quantum dots is presented. Magnetic fields are applied in the growth direction of the semiconductor heterostructure. The parity of the excitonic envelope function related to the simultaneous exchange of $z_e \rightarrow -z_e$ and $z_h \rightarrow -z_h$ is a good quantum number and the wave function, both the odd and even parity, can be expanded as combination of products of the quantum well electron and hole function that preserves the parity with appropriate Gaussian functions. We have simultaneously obtained the energies of the excitonic ground and excited states and discuss the behavior of these energies as a function of the magnetic field.

PACS. 71.35.Cc Intrinsic properties of excitons; optical absorption spectra – 71.35.Ji Excitons in magnetic fields; magnetoexcitons – 71.55.Eq III-V semiconductors – 78.66.Fd III-V semiconductors

1 Introduction

The quantitative understanding of the physics of low-dimensional semiconductor systems is of paramount importance due to its potential applications in electronic and optoelectronic devices. In that respect, the study of the electronic and excitonic properties of semiconductor heterostructures is of great interest, and the quest for an appropriate and reliable knowledge of the excitonic and optical properties of single and multiple semiconductor quantum wells (QWs), quantum-well wires (QWWs), quantum dots (QDs), superlattices (SLs), self-assembled quantum dots (SAQDs), etc., has resulted in a considerable amount of work in order to elucidate the physical properties of these systems [1–25]. External influences such as applied electric and magnetic fields [1–3], and effects of hydrostatic pressure [4–6] have been measured and/or calculated. Studies include one-particle states [7,8], exciton and biexciton states [9–25], analytic forms of the linear and third-order nonlinear optical absorption coefficients, diamagnetic shift, absorption spectra, etc. Nonlocal dynamic response and level crossings, and acceptor levels in QDs, as well as QD/interface defects in narrow QWs have also been reported [19–21]. Some of the conclusions are that (i) as a result of the applied electric and magnetic fields in QWs, there is an infrared shift in the optical absorption spectra and Stark/Landau ladder

anticrossings [1]; (ii) type II electron-hole recombinations can be obtained by hydrostatic pressure in those systems in which, in the atmospheric pressure regime, the transitions go as type I [4,5]; (iii) Pacheco and Barticevic [7] concluded that for QDs under applied electric fields and in the weak-lateral confinement regime, the electron-hole system is appropriately described by the relative and center-of-mass coordinates, which are weakly coupled by the lateral potential; and in the strong-lateral confinement regime the electrons and holes are weakly correlated and the spectrum may be explained within a single-particle picture; (iv) associated with geometrical-confinement effects in QDs, there is a strong blue-shift of the luminescence [13]; (v) the energies of the excitonic states in QDs – and the interval between them – decrease with reducing space dimensions [17]; (vi) the optical absorption saturation intensity in QDs may be controlled by adopting a proper parabolic confinement potential [18]; (vii) the spin relaxation can be strongly suppressed in SAQDs [22].

In the last decade or so, there has been much interest in the physical understanding of semiconductor SAQDs, both from the experimental and theoretical points of view [19–25]. In particular, here we are concerned with the physical understanding of the excitonic and optical properties of SAQDs, and perform a thorough theoretical study of a number of properties of GaAs-Ga_{1-x}Al_xAs single QDs. To our knowledge, many questions remain open today on the optical transitions in QDs. In SAQDs

^a e-mail: cduque@fisica.udea.edu.co

there is no conclusive answers on the number of electron states that contribute to the photoluminescence spectra. Another open question corresponds to the excitonic effects in these dots: when the $e-h$ Coulomb interaction is taken into account, anticrossing effects between different electron-hole states should be observed. There are no studies that clearly discuss the anticrossing between excitonic states in QDs, particularly when external magnetic fields effects are considered. In the present work we use the effective-mass approximation to describe the correlated electron-hole pair in GaAs-Ga_{1-x}Al_xAs QDs. The model considers a thin QW that confines the carries in the z -direction. For the $x-y$ in-plane confinement, we consider an infinite parabolic potential, and the externally applied magnetic field is taken along the growth direction of the heterostructure. The work is organized as follows. In Section 2 we present the theoretical framework, Section 3 is devoted to the present results and discussion, and finally in Section 4 we present our conclusions.

2 Theoretical framework

The effective-mass Hamiltonian for a disk-shaped GaAs-Ga_{1-x}Al_xAs QD, in the presence of a magnetic field B applied along the z -growth direction, is given by the sum of single-particle Hamiltonians for electron and hole, the dot potential that confines the carries inside the heterostructure, and the $e-h$ Coulomb potential screened by a dielectric constant,

$$H = H_e + H_h + V_{\text{Dot}} + V_C, \quad (1)$$

where

$$H_e = -\frac{\hbar^2}{2m_e^*} \frac{\partial^2}{\partial z_e^2} + \frac{1}{2m_e^*} \left[-i\hbar(\nabla_e)_{\parallel} + \frac{e}{c} \vec{A}(\vec{r}_e) \right]^2, \quad (2)$$

$$H_h = -\frac{\hbar^2}{2m_{h\perp}^*} \frac{\partial^2}{\partial z_h^2} + \frac{1}{2m_{h\parallel}^*} \left[-i\hbar(\nabla_h)_{\parallel} - \frac{e}{c} \vec{A}(\vec{r}_h) \right]^2, \quad (3)$$

$$V_{\text{Dot}} = \frac{1}{2}m_e^* \omega_e^2 \rho_e^2 + \frac{1}{2}m_{h\parallel}^* \omega_h^2 \rho_h^2 + V_e(z_e) + V_h(z_h), \quad (4)$$

and

$$V_C = -\frac{e^2}{\epsilon \sqrt{(\vec{\rho}_e - \vec{\rho}_h)^2 + (z_e - z_h)^2}}. \quad (5)$$

Note that the above QD confinement potential has been modelled by the sum of a lateral parabolic potential and a one-dimensional square-well potential along the growth direction. We assume the square-well potential barriers [26] $V_e(z_e)$ and $V_h(z_h)$ to be 62% (38%) of the band-gap discontinuity [27] ΔE_g (eV) = 1.36 x + 0.22 x^2 for the conduction (valence) band, with the GaAs gap taken as the low-temperature [27] value $E_g = 1.5194$ eV. To solve the eigenvalue problem for the Hamiltonian in (1), we take the vector potential in the symmetric gauge as

$\vec{A} = (B/2)(-y, x, 0)$, use relative ($\vec{\rho}$) and center-of-mass (CM) (\vec{R}) coordinates for in-plane motion, and obtain

$$\begin{aligned} H = & -\frac{\hbar^2}{2\eta} \nabla_R^2 + \frac{1}{2} \eta \omega_{CM}^2 R^2 \\ & -\frac{\hbar^2}{2\mu} \nabla_{\rho}^2 + \frac{1}{2} \mu \omega^2 \rho^2 + \frac{1}{2} \mu \left(\frac{1}{4} \omega_c^2 \right) \rho^2 \\ & + \mu (\omega_e^2 - \omega_h^2) \vec{\rho} \cdot \vec{R} + \frac{eB}{2c} \left(\frac{1}{m_e^*} - \frac{1}{m_{h\parallel}^*} \right) \ell_z \\ & -\frac{\hbar^2}{2m_e^*} \frac{\partial^2}{\partial z_e^2} - \frac{\hbar^2}{2m_{h\perp}^*} \frac{\partial^2}{\partial z_h^2} + V_e(z_e) \\ & + V_h(z_h) - \frac{e^2}{\epsilon \sqrt{\rho^2 + (z_e - z_h)^2}}, \end{aligned} \quad (6)$$

where $\omega_c = eB/(\mu c)$, $\ell_z = -i\hbar(x\partial/\partial y - y\partial/\partial x)$, $\mu = m_e^* m_{h\parallel}^* / (m_e^* + m_{h\parallel}^*)$, $\eta = m_e^* + m_{h\parallel}^*$, and the characteristic frequencies ω_{CM} and ω are given by

$$\omega_{CM}^2 = (m_e^* \omega_e^2 + m_{h\parallel}^* \omega_h^2) / \eta \quad (7)$$

and

$$\omega^2 = (m_{h\perp}^* \omega_e^2 + m_e^* \omega_h^2) / \eta. \quad (8)$$

The z -dependent confinement potential, $V(z)$, is invariant under the transformation $z \rightarrow -z$. Therefore, one may assign a definite parity for the e or h QW wave function. As the $e-h$ Coulomb interaction is invariant under the simultaneous inversion of the electron and hole positions, the exciton envelope wave function will therefore have a well-defined parity (i.e., parity is a good quantum number), and the excitonic envelope function may be expanded as products of QW electron and hole eigenfunctions preserving the parity. Then we can write

$$\begin{aligned} \Psi^{\pm}(\vec{\rho}, \vec{R}, z_e, z_h) = & \sum_{P, P'} \sum_{n_e(P), n_h(P')} C^{n_e(P), n_h(P'), (\pm)}(\vec{\rho}, \vec{R}) \\ & \times f_{n_e(P)}(z_e) f_{n_h(P')}(z_h) \Delta_{P, P'}, \end{aligned} \quad (9)$$

where P, P' indicates even or odd parity, and $\Delta_{P, P'} = \delta_{P, P'}$ for even (+) excitonic states, whereas $\Delta_{P, P'} = (1 - \delta_{P, P'})$ for odd (-) states. In the above, $f_{n_e(P)}(z_e)$ and $f_{n_h(P')}(z_h)$ are the QW electron and hole eigensolutions, respectively, i.e.,

$$\left(-\frac{\hbar^2}{2m_e^*} \frac{\partial^2}{\partial z_e^2} + V_e(z_e) \right) f_{n_e(P)} = (E_e + E_g) f_{n_e(P)} \quad (10)$$

and

$$\left(-\frac{\hbar^2}{2m_{h\perp}^*} \frac{\partial^2}{\partial z_h^2} + V_h(z_h) \right) f_{n_h(P)} = E_{hh} f_{n_h(P)}. \quad (11)$$

By ignoring the coupling between the in-plane relative and CM coordinates [7], one may write the $C^{n_e(P), n_h(P'), (\pm)}$

coefficient as products of the in-plane and CM eigensolutions, i.e.,

$$C^{n_e(P), n_h(P'), (\pm)}(\rho, \theta, R, \Theta) = B^{n_e(P), n_h(P'), (\pm)}(\rho, \theta) g_{l,n}(R, \Theta), \quad (12)$$

where $g_{l,n}(R, \Theta)$ is the eigenfunction of the CM Hamiltonian, which corresponds to a bi-dimensional harmonic oscillator, i.e.,

$$\left(-\frac{\hbar^2}{2\eta} \nabla_R^2 + \frac{1}{2} \eta \omega_{CM}^2 R^2 \right) g_{l,n}(R, \Theta) = \hbar \omega_{CM} (n+1) g_{l,n}(R, \Theta) \quad (13)$$

with

$$g_{l,n}(R, \Theta) = e^{il\Theta} R^{|l|} e^{-\left(\frac{\eta \omega_{CM}}{2\hbar} R^2\right)} L_{(n-|l|)/2}^{|l|} \left(\frac{\eta \omega_{CM}}{\hbar} R^2 \right). \quad (14)$$

With all the above-mentioned, we obtain the following eigenvalue equation for $B^{n_e(P), n_h(P), (+)}(\rho, \theta)$ ([and a similar equation for the $(-)$ solution]):

$$\left[-\frac{\hbar^2}{2\mu} \nabla_\rho^2 + \frac{1}{2} \mu \omega_{eff}^2 \rho^2 + \frac{eB}{2c} \left(\frac{1}{m_e^*} - \frac{1}{m_h^*} \right) \ell_z - \varepsilon(n_e(P), n_h(P)) + \hbar \omega_{CM} (n+1) \right] B^{n_e(P), n_h(P), (+)}(\rho, \theta) - \sum_{P'} \sum_{n_e(P'), n_h(P')} V_{n_e(P), n_h(P)}^{n_e(P'), n_h(P')}(\rho) \times B^{n_e(P'), n_h(P'), (+)}(\rho, \theta) = 0, \quad (15)$$

where

$$\varepsilon(n_e(P), n_h(P)) = E_{exc} - E_e - E_{hh} - E_g, \quad (16)$$

$$\omega_{eff} = \sqrt{\omega^2 + \frac{1}{4} \omega_c^2}. \quad (17)$$

and

$$V_{n_e(P), n_h(P)}^{n_e(P'), n_h(P')}(\rho) = \left\langle f_{n_e(P)}(z_e) f_{n_h(P)}(z_h) | V_C | f_{n_e(P')} (z_e) f_{n_h(P')} (z_h) \right\rangle. \quad (18)$$

We note that the above matrix element is θ -independent, equation (15) has azimuthal-symmetry and therefore one may write

$$B^{n_e(P), n_h(P), (+)}(\rho, \theta) = \exp(im\theta) F_{n_e(P), n_h(P)}^{(+, m)}(\rho), \quad (19)$$

i.e., the z -component of the angular momentum is a good quantum number. By substituting (19) into (15), we then obtain a set of coupled equations for $F_{n_e(P), n_h(P)}^{(+, m)}(\rho)$, which may be solved numerically by expanding $F^{(+, m)}$

in a set of Gaussian-type functions with length parameters λ , chosen in order to cover the physical range of relevant spatial parameters [7]. In order to obtain accurate energies and wave functions, we have used a truncated basis up to 900 states. We use a set of 25 Gaussian functions with parameters λ covering the range from 1 Å to 5000 Å, and with a maximum of 18 $e-h$ QW functions with the same parity (even-exciton solutions) and a maximum of 18 $e-h$ QW functions with opposite parity (odd-exciton solutions).

3 Results and discussion

The dimensions of the QD are modelled as follows: the lateral QD radius was taken as $R = \sqrt{\hbar/\mu\omega}$, where μ is the in-plane heavy-hole exciton effective mass, whereas the height of the dot corresponds to the L_z width of a QW in the z -direction. Moreover, the $e-h$ Coulomb interaction is screened by the $\epsilon = 12.4$ static dielectric constant [27] of the GaAs, i.e., image-charge effects are ignored. Relevant mass parameters are taken from the work by Li [27]. Calculations were performed for $P = P'$ (cf. Eq. (9)), i.e., results presented are for even excitons (one may show that the odd-exciton peaks would be associated to much higher PL-peak energies). In our model the energy spectrum for the $e-h$ non-interacting pair in a QD has energy sequences of Landau-like levels (see, for instance, Figs. 1a and 2a) associated with the various non-correlated $e-h$ states in a QW/QD of width L_z . Also, one should notice that as the relative motion of the carriers and that of the center of mass are taken as independent, then the Coulomb interaction only mixes states with the same m . Moreover, in the absence of external magnetic fields, the Hamiltonian depends on the absolute value of m and for it the energies are degenerate for states with angular moment equal to $\pm m$. Finally, energy levels $E_{M,m}$ in the present work are labelled as (M,m), which is strictly valid only for the case of a non-interacting $e-h$ pair, where m is the azimuthal quantum number in (19), and M is associated with the energy level of the bi-dimensional harmonic oscillator spectrum (cf. Eqs. (6) and (8)), i.e., $E_{M,m} = \hbar\omega(M+1)$, with $M \geq 0$, $-M \leq m \leq M$, and m and M are either both even or both odd [28].

In Figure 1, we present our results for the heavy-hole exciton peak, which would show up in experiment, for instance, as a photoluminescence peak, and for the correlation energies (here defined as the $e-h$ Coulomb-interaction energy) for a GaAs-Ga_{0.7}Al_{0.3}As QD of thickness $L_z = 10$ Å and for zero magnetic field. Figure 1a shows the excitonic peak as a function of the lateral confining energy and for this ultrathin QW only one set of peaks can be observed. For low-lateral confinement energies ($\hbar\omega \ll R_x^*$, where R_x^* is the QW exciton effective Rydberg) the spectrum manifest excitonic character, as it is clearly seen for the ground-state (gs) exciton: in Figure 1a, the energy position of the gs exciton peak essentially goes to the appropriate limiting value of $E_g + E_e + E_{hh} - R_x^* + \mu\omega^2/2\langle\rho^2\rangle$, and in Figure 1c the

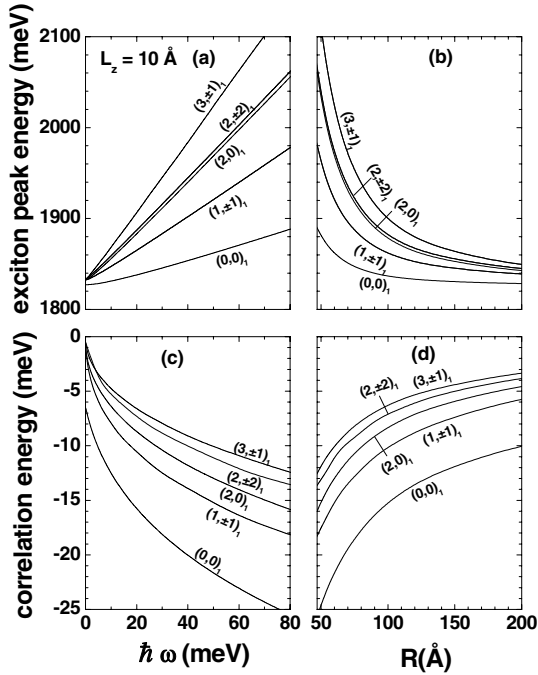


Fig. 1. Heavy-hole exciton peak [(a) and (b)] and correlation energies [(c) and (d)] for a disk-shaped GaAs-Ga_{0.7}Al_{0.3}As QD of thickness $L_z = 10$ Å, and lateral radius R , as functions of the strength $\hbar\omega$ of the in-plane confinement potential [(a) and (c)] or lateral disk radius $R = \sqrt{\hbar/\mu\omega}$ [(b) and (d)], where μ is the heavy-hole exciton effective mass.

gs correlation energy behaves, in the low-lateral confining regime, as $-R_x^* - \hbar\omega(M+1) + \mu\omega^2/2\langle\rho^2\rangle$. As the $\hbar\omega$ confining energy increases, one eventually reaches the harmonic oscillator regime, in which the exciton peak energy behaves, in this limit, as $\hbar\omega(M+1)$, as expected (cf. Fig. 1a). Moreover, the exciton binding energy (defined as the negative of the correlation energy) behaves, for $\hbar\omega \gg R_x^*$, as $\approx 1/R \approx \sqrt{\omega}$ as seen in Figures 1c and 1d. Note that, in this regime, the electron and hole are strongly confined in the z -direction and, although the Coulomb interaction may be considered as a perturbation, the behavior of the exciton binding energy is essentially governed by the effect of the $e-h$ Coulomb interaction energy on the energy harmonic-oscillator states. Figures 1b and 1d display the exciton spectrum and correlation energies as functions of the corresponding lateral QD radius, respectively. It is apparent that for QD radii larger than the effective Bohr radius ($a_0^* \approx 150$ Å), the excitonic spectrum and correlation energies are essentially independent of the lateral confinement energy, as expected.

In Figure 2 we display both the non-interacting (non-correlated) $e-h$ pair energies and the excitonic peak energies for a GaAs-Ga_{0.7}Al_{0.3}As QD of thickness $L_z = 50$ Å and zero magnetic field, as functions of the strength of the lateral confining potential. This allows one to identify, as the lateral confinement increases, the possible occurrence of energy crossings/anticrossings, when the effect of the Coulomb interaction is taken into account in the calculation of the corresponding excitonic states. For the QW

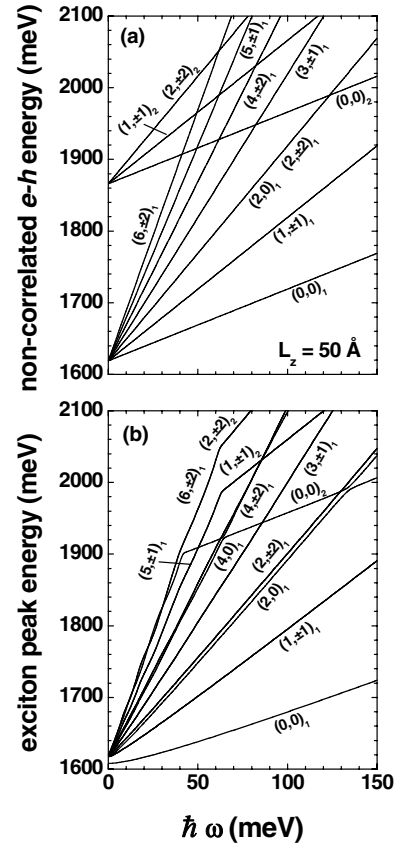


Fig. 2. Non-correlated electron-heavy-hole ($e-h$) (a) and corresponding exciton peak energies (b) for a disk-shaped GaAs-Ga_{0.7}Al_{0.3}As QD of thickness $L_z = 50$ Å, and lateral radius $R = \sqrt{\hbar/\mu\omega}$, as functions of the strength $\hbar\omega$ of the in-plane confinement potential.

width $L_z = 50$ Å, the $e-h$ non interacting pair shows two manifolds of energy levels associated with the two possible z -confined $e-h$ QW states of the same parity, with each manifold associated with a bi-dimensional harmonic oscillator spectrum. Note the crossing of the uncorrelated energy states when the lateral confining strength is varied. Of course, the crossing position of noninteracting $e-h$ states provides information on the comparative strength of lateral and QW confinement energies. Also, one should notice that the Coulomb interaction only couples exciton states with the same azimuthal quantum number m and it is such $e-h$ interaction that produces the level anticrossings observed in Figure 2b.

In Figure 3a, we present our results for even-parity excitonic peak energies for the low-energy excitonic states with the z -component of angular momentum, m , running from -2 to 2 , as functions of the lateral confinement energy of $L_z = 100$ Å GaAs-Ga_{0.7}Al_{0.3}As QDs, at zero magnetic field. The energy spectrum shows exciton states originated from three different manifolds associated to QW $e-h$ z -confined states. For clarity, we display in Figure 3b only $m = 0$ excitonic states, which can be optically excited with circularly-polarized light. Again, experimental measurements around the anticrossing region will provide

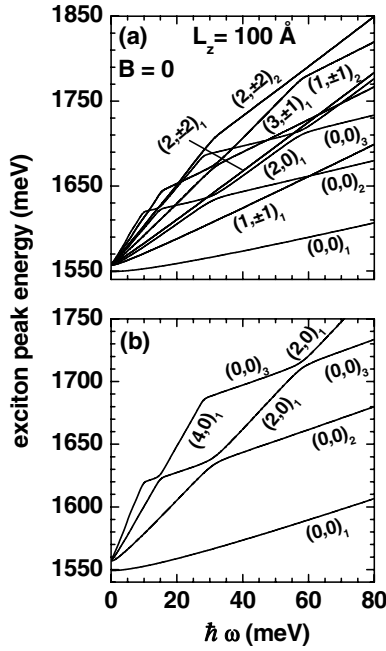


Fig. 3. Excitonic peak energies for the lower even parity excitonic states with the z -component of angular momentum, m , running from -2 to 2 , as a function of the lateral confinement energy in the case of a GaAs-Ga_{0.7}Al_{0.3}As QD of thickness $L_z = 100$ Å and lateral radius $R = \sqrt{\hbar/\mu\omega}$, at zero magnetic field. In (b) only excitonic energies with $m = 0$ are displayed.

information of the comparative value of the lateral and QW confinement. Of course, the same information could be experimentally obtained in a much easier way by probing the semiconductor QD system by a variable growth-direction magnetic field.

Figure 4 displays the magnetic-field effects on the excitonic peak energies in a GaAs-Ga_{0.7}Al_{0.3}As QD of thickness $L_z = 100$ Å and radius $R = 100$ Å. In Figure 4a, we present calculated results for excitonic peak energies for the lower excitonic states for the azimuthal quantum number m running from -2 to $+2$ as functions of the magnetic field. As before, results are shown for exciton states originated from three different manifolds associated to QW $e - h$ z -confined states. The applied magnetic field lifts the energy degeneracy in the quantum number m and yields to a rich-structured spectrum. In Figure 4b, only excitonic energies with $m = 0$ are displayed as a function of the magnetic field, so that one clearly observes the anticrossing of exciton levels associated to the three lowest QW z -confined manifold. An estimate of the value of the magnetic field for which the anticrossing occurs may be calculated as follows. For instance, the anticrossing of the $(2,0)_1$ and $(0,0)_2$ levels is given by $E_{(2,0)_1} \approx E_{(0,0)_2}$, i.e., $E_{QW,1} + 3\hbar\omega_{eff} \approx E_{QW,2} + \hbar\omega_{eff}$, where $\omega_{eff}^2 = \omega^2 + \omega_c^2/4$, and $E_{QW,1}$ and $E_{QW,2}$ are two different solutions, with the same parity, of the QW $e - h$ z -confined states. In order to see how the anticrossings depend on parameters, we have also displayed in Figures 4c and 4d our calculated results when R changes from 100 Å to 150 Å (Fig. 4c) or when L_z changes from 100 Å to

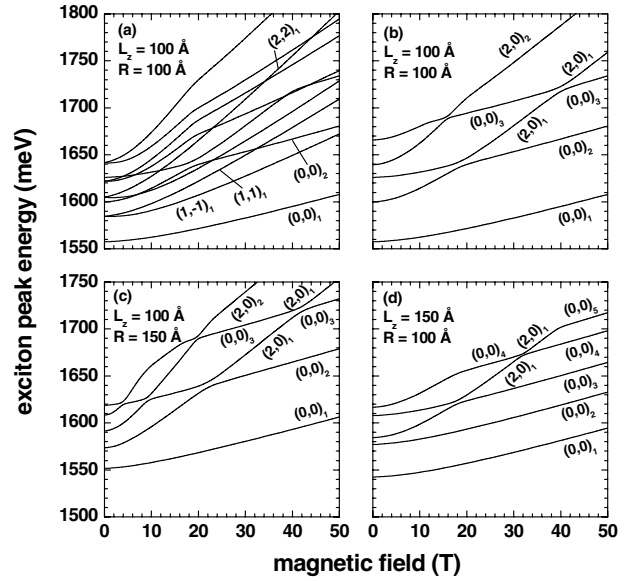


Fig. 4. (a) Excitonic peak energies for the lower even parity excitonic states with the z -component of angular momentum, m , running from -2 to 2 , as a function of the growth-direction applied magnetic field in the case of a GaAs-Ga_{0.7}Al_{0.3}As QD of thickness $L_z = 100$ Å, and radius $R = 100$ Å. In (b) only excitonic energies with $m = 0$ are displayed; (c) as in (b), for $L_z = 100$ Å, and radius $R = 150$ Å; (d) as in (b), for $L_z = 150$ Å, and radius $R = 100$ Å.

150 Å (Fig. 4d). In general the anticrossings widths will be larger for higher excitonic confinement as it can be observed in Figure 4b as compared with Figure 4d. However in the case of similar z -confinement but different geometric lateral-confinement as in Figures 4b and 4c the anticrossing width is found to be nearly the same. This is because the lower lateral geometric confinement in the last case is compensated by a higher magnetic-field confinement because the anticrossings occur for larger field values.

In Figure 5, the calculated binding energies of the ground state in disk-shaped GaAs-Ga_{0.7}Al_{0.3}As QDs, as functions of the QD lateral radius, are presented. Different values of the height of the dot and of the applied magnetic field are considered. One notes from Figure 5 that, for small QD lateral radii, i.e., $R \sim 50$ Å, the effects of applied magnetic fields are quite visible, even for fields of the order of 20 – 40 T. In the high confinement regime and zero magnetic field, when the dot radius increases, the exciton binding energy decreases as approximately $1/R$. In the opposite regime, i.e., when the Coulomb interaction is predominant over the lateral confinement, the binding energy should be essentially constant as the dot radius increases. The insets show that for the large radius limit, the exciton binding energy behaves as \sqrt{B} in agreement with the predominant effect of the magnetic confinement. In this case, the $e - h$ pair essentially does not feel the effects of either the QW barriers or of the lateral parabolic potential.

Finally, in Figure 6 we present the exciton ground-state peak energy for different configurations (L_z , R_{QD}) of the

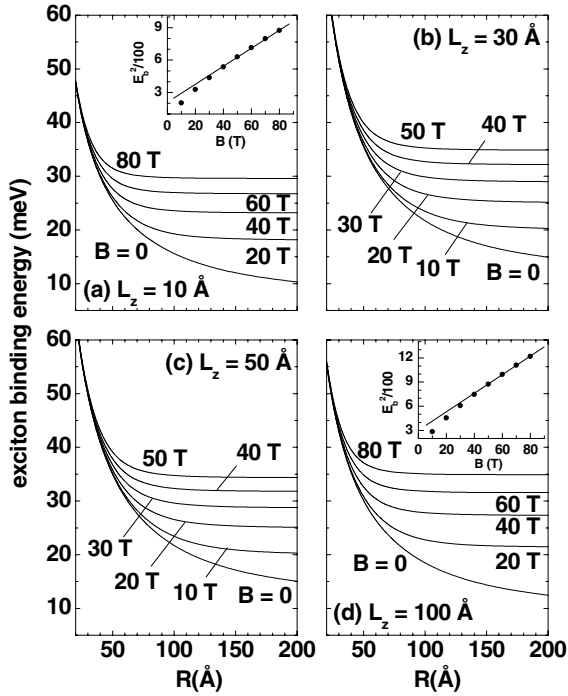


Fig. 5. Heavy-hole exciton binding energies for a disk-shaped GaAs-Ga_{0.7}Al_{0.3}As QD of thicknesses (a) $L_z = 10$ Å, (b) $L_z = 30$ Å, (c) $L_z = 50$ Å, and (d) $L_z = 100$ Å, as functions of the disk radius R , and different values of the growth-direction applied magnetic field. Insets in (a) and (d) show the magnetic-field dependence of the square of the exciton binding energy (E_b^2) in the limit of large QD radii (full dots are theoretical values, and the line indicates the linearity for large values of the magnetic field).

QD. In order to zoom in the effects of the applied magnetic field, in part (b) the diamagnetic shift [$E(B) - E(0)$, where $E(B)$ is the applied magnetic field dependent exciton peak energy] is presented. Clearly it is observed that for small values of the applied magnetic field (up to 20 T) and high radial confinement ($R_{QD} = 50$ Å) the diamagnetic shift shows a quadratic dependence with the magnetic field, just as it has been observed by Itskevich et al. [4] in self-assembled InAs/GaAs QDs with dimensions in the order of magnitude of 100 Å, where the electron and/or hole wave functions are strongly confined. For higher fields, the diamagnetic shift behaves linearly with the field, what demonstrates the decrease of the effect of the potential barriers since the system is acquiring the lineal character with the magnetic field of in bulk Landau levels. For weak radial confinement ($R_{QD} = 100$ Å) the high dependence with the magnetic field is observed since the wave functions are quite extended in the space and they are more susceptible to the radial magnetic confinement as effect of the applied magnetic fields.

4 Conclusions

In summary, we have studied the excitonic spectra of disk-shaped QDs, subject to an uniform magnetic field, applied

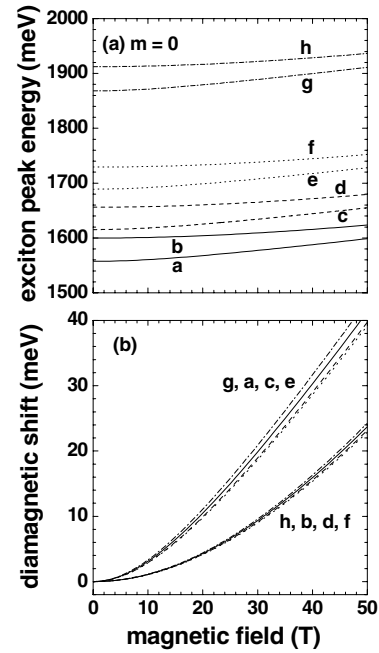


Fig. 6. Heavy-hole $m = 0$ exciton peak energy (a) and diamagnetic shift of the exciton energy (b) as a function of the z -direction applied magnetic field, for disk-shaped GaAs-Ga_{0.7}Al_{0.3}As QDs of thicknesses L_z and lateral disk radii R . Different dot dimensions (L_z, R) are considered: (a) (100 Å, 100 Å), (b) (100 Å, 50 Å), (c) (50 Å, 100 Å), (d) (50 Å, 50 Å), (e) (30 Å, 100 Å), (f) (30 Å, 50 Å), (g) (10 Å, 100 Å), and (h) (10 Å, 50 Å).

along the QD axis. We obtain the excitonic ground state and the excited states simultaneously, with calculated results displaying the appropriate physical behavior. The parity of the excitonic envelope function related to the simultaneous exchange of $z_e \rightarrow -z_e$ and $z_h \rightarrow -z_h$ is a good quantum number, and the exciton wave function (both the odd and even parity functions) can be expanded as a combination of products of the QW electron and hole functions that preserves the parity. The Coulomb interaction only couples excitons with the same m and the same parity, and it is this coupling that turns crossings of levels into level anticrossings [29].

If one is able to observe the anticrossing region, it will provide information on the relative values of the lateral and axial confinements. Anticrossing effects can be detected by optical techniques like photoluminescence and photocurrent spectroscopy [30,31]. Of course, the lateral confinement may be varied by applying a magnetic field in the axial direction, and, experimentally, these excitons may be optically excited with circularly-polarized light. Here we must mention that to perform high magnetic-field measurements of diamagnetic shifts is a notoriously difficult task [32–34] and therefore trying to infer information on band-structure or QD energy levels must be viewed with care. Nevertheless, we do believe the present theoretical findings provide results for the magnetic-field dependence of the excitonic spectrum of a disk-shaped QD with different geometrical configurations which may be valuable in analyzing future experimental studies.

This research was partially supported by Colombian COLCIENCIAS, CODI-Universidad de Antioquia Agencies, CONICYT/COLCIENCIA N° 2005 - 207 and by the Excellence Center for Novel Materials/COLCIENCIAS (contract No. 043-2005). We also acknowledge Chilean support by PBCCT - ACT027, Fondecyt (grants 1061237 and 7070292), Universidad Técnica Federico Santa María (internal grant), and Brazilian Agencies CNPq, FAPESP, Rede Nacional de Materiais Nanoestruturados/CNPq, and Millenium Institute for Quantum Computing/MCT.

References

1. M. Pacheco, Z. Barticevic, F. Claro, J. Phys.: Condens. Matter **5**, A363 (1993); Z. Barticevic, M. Pacheco, F. Claro, Phys. Rev. B **51**, 14414 (1995); M. Pacheco, Z. Barticevic, Phys. Rev. B **64**, 033406 (2001)
2. K.L. Janssens, F.M. Peeters, V.A. Schweigert, Phys. Rev. B **63**, 205311 (2001)
3. Z. Barticevic, M. Pacheco, C.A. Duque, L.E. Oliveira, J. Phys.: Condens. Matter **14**, 1021 (2002)
4. I.E. Itskevich, S.G. Lyapin, I.A. Troyan, P.C. Klipstein, L. Eaves, P.C. Main, M. Henini, Phys. Rev. B **58**, R4250 (1998); I.E. Itskevich, M.S. Skolnick, D.J. Mowbray, I.A. Troyan, S.G. Lyapin, L.R. Wilson, M.J. Steer, M. Hopkinson, L. Eaves, P.C. Main, Phys. Rev. B **60**, R2185 (1999)
5. B.S. Ma, X.D. Wang, F.H. Su, Z.L. Fang, K. Ding, Z.C. Niu, G.H. Li, J. Appl. Phys. **95**, 933 (2004)
6. C.A. Duque, N. Porrás-Montenegro, Z. Barticevic, M. Pacheco, L.E. Oliveira, Microelectr. J. **36**, 231 (2005)
7. M. Pacheco, Z. Barticevic, Phys. Rev. B **55**, 10688 (1997)
8. O. Stier, M. Grundmann, D. Bimberg, Phys. Rev. B **59**, 5688 (1999); A.J. Williamson, L.W. Wang, A. Zunger, Phys. Rev. B **62**, 12963 (2000)
9. D.G. Austing, S. Sasaki, S. Tarucha, S.M. Reimann, M. Koskinen, M. Manninen, Physica B **272**, 68 (1999)
10. K. Hirose, N.S. Wingreen, Phys. Rev. B **59**, 4604 (1999)
11. A. Wojs, P. Hawrylak, S. Fafard, L. Jacak, Phys. Rev. B **54**, 5604 (1996)
12. A.H. Rodríguez, C. Trallero-Giner, S.E. Ulloa, J. Marín-Antuña, Phys. Rev. B **63**, 125319 (2001)
13. J. Song, S.E. Ulloa, Phys. Rev. B **52**, 9015 (1995)
14. W. Xie, Physica B **279**, 253 (2000)
15. R. Nötzel, U. Jahn, Z. Niu, A. Trampert, J. Fricke, H.-P. Schönherr, T. Kurth, D. Heitmann, L. Däweritz, K.H. Ploog, Appl. Phys. Lett. **72**, 2002 (1998)
16. M. Bayer, S.N. Walck, T.L. Reinecke, A. Forchel, Phys. Rev. B **57**, 6584 (1998)
17. W. Xie, Physica B **358**, 109 (2005)
18. G. Wang, K. Guo, Physica E **28**, 14 (2005)
19. T. Demel, D. Heitmann, P. Grambow, K. Ploog, Phys. Rev. Lett. **64**, 788 (1990)
20. M. Pacheco, Z. Barticevic, J. Phys.: Condens. Matter **11**, 1079 (1999)
21. Z. Barticevic, M. Pacheco, C.A. Duque, L.E. Oliveira, Phys. Rev. B **68**, 073312 (2003)
22. A. Kuther, M. Bayer, A. Forchel, A. Gorbunov, V.B. Timofeev, F. Schäfer, J.P. Reithmaier, Phys. Rev. B **58**, R7508 (1998)
23. M. Braskén, M. Lindberg, D. Sundholm, J. Olsen, Phys. Rev. B **61**, 7652 (2000)
24. A. Lorke, J.P. Kotthaus, K. Ploog, Phys. Rev. Lett. **64**, 2559 (1990)
25. J.J. Palacios, P. Hawrylak, Phys. Rev. B **51**, 1769 (1995); B. Partoens, F.M. Peeters, Phys. Rev. Lett. **84**, 4433 (2000)
26. W. Wang, E.E. Mendez, F. Stern, Appl. Phys. Lett. **45**, 639 (1984)
27. E.H. Li, Physica E **5**, 215 (2000)
28. C. Cohen-Tannoudji, B. Diu, F. Laloë, in *Quantum Mechanics*, Complement D-VI (Hermann and John Wiley and Sons, Paris, 1977)
29. The absence of the inversion symmetry in the z -potential does not produced fundamental changes in the obtained results. In this case, if the Coulomb interaction is not considered, there are also electron-hole wave functions formed by different states of independent particles (of course these states will not have definite parity) and subbands associated to each $e-h$ pairs with different quantum numbers in z . The exciton energies as a function of the magnitude of an in-plane magnetic field will show anticrossings between subbands levels due to the electron-hole coupling
30. A.M. Fox, D.A.B. Miller, G. Livescu, J.E. Cunningham, W.Y. Jan, Phys. Rev. B **44**, 6231 (1991)
31. A. Alexandrou, E.E. Mendez, J.M. Hong, Phys. Rev. **44**, 1934 (1991)
32. A. Rastelli, S. Stuffer, A. Schliwa, R. Songmuang, C. Manzano, G. Constantini, K. Kern, A. Zrenner, D. Bimberg, O.G. Schmidt, Phys. Rev. Lett. **92**, 166104 (2004)
33. N. Schildermans, M. Hayne, V.V. Moshchalkov, A. Rastelli, O.G. Schmidt, Phys. Rev. B **72**, 115312 (2005)
34. Y. Sidor, B. Partoens, F.M. Peeters, N. Schildermans, M. Hayne, V.V. Moshchalkov, A. Rastelli, O.G. Schmidt, Phys. Rev. B **73**, 155334 (2006)